Case Report

Undifferentiated carcinoma of the pancreas with osteoclast-like giant cells showing intraductal growth and intratumoral hemorrhage: MRI features

Keisuke Sato, MD[a], Hiroshi Urakawa, MD[a], Keiko Sakamoto, MD[a], Emi Ito, MD[a], Yoshihiro Hamada, MD[b], Kengo Yoshimitsu, MD, PhD[a],*

[a] *Department of Radiology, Fukuoka University Faculty of Medicine, Fukuoka University, 7-45-1 Nanakuma, Jonan-ku, Fukuoka-shi, Fukuoka 814-0180, Japan*
[b] *Department of Pathology, Fukuoka University Faculty of Medicine, Fukuoka University, 7-45-1 Nanakuma, Jonan-ku, Fukuoka-shi, Fukuoka 814-0180, Japan*

ARTICLE INFO

ABSTRACT

We report a case of undifferentiated carcinoma of the pancreas with osteoclast-like giant cells ocalized within the main pancreatic duct (MPD). A 61-year-old woman was referred to our hospital for evaluation of dilatation of the MPD that was detected on screening sono-gram. Preoperative MR imaging revealed a small hypervascular tumor within the dilated MPD, showing high signal on R2* map and signal reduction on in-phase as compared to out-of-phase. R2* hyperintensity and in-phase signal reduction may be a characteristic fea-ture of undifferentiated carcinoma of the pancreas with osteoclast-like giant cells, which indicates intratumoral hemorrhage even if they are small.

Case report

A 61-year-old Japanese woman was referred to our hospital for further investigation of dilatation of the main pancreatic duct (MPD). Her past history included type-2 diabetes mellitus, hypertension, hyperlipidemia, hyperuricemia, gall bladder stone with adenomyomatosis, and fatty liver. She had been mostly asymptomatic and periodical screening ultrasonography (US) examination incidentally revealed dilated MPD. Screening US performed 2 years earlier was negative. Her family history was unremarkable. Laboratory data on admission was unremarkable, including serum amylase level, except for slightly elevated serum glucose (118 mg/dL) and HbA1c (6.8 %). IgG4 and tumor makers including carcinoembryonic antigen, carbohydrate antigen 19-9, and DUPAN-2 were all negative.

Computed tomography (CT) revealed a polypoid lesion occupying the MPD lumen, measuring approximately 40 mm in length at the pancreas head and body. No calcification was seen. The major part of the lesion in the MPD of the pancreatic body showed apparent enhancement on the arterial dominant phase and subsequent washout on the equilibrium phase, but the part of the lesion in the MPD of the pancreatic head was weakly enhanced both on arterial phase and equilibrium phase (Fig. 1). The parenchyma of the pancreatic tail showed slight atrophy and prolonged enhancement with a dilated MPD, suggesting obstructive pancreatitis. Magnetic resonance imaging (MRI) using a 3 T MR system (Discovery MR750w 3.0 T, GE Healthcare, Milwaukee, WI) was performed for the pancreas lesion. On T2-weighted images (Fig. 2A) and diffusion-weighted image (not shown), the tumor was markedly hypointense. On R2* map obtained by iterative decomposition of water and fat with echo asymmetry and least-squares estimation (IDEAL) IQ, the tumor was hyperintense with mean R2* value of approximately 300 per second (Fig. 2B). The tumor showed apparent signal reduction on in-phase as compared to out-of-phase image of chemical shift MRI (Fig. 2C and D). The lesion exhibited intraluminal location within MPD, and the intraparenchymal component

was hardly appreciated either on CT or MRI. The Fluorine 18-Fluorodeoxyglucose positron emission tomography combined with CT (18F-FDG-PET/CT) showed uptake of FDG at the pancreas lesion with the maximum standardized uptake value of 4.03 and no evidence of metastasis (Fig. 3). Endoscopic retrograde pancreatography and intraductal US demonstrated the tumor within MPD. Preoperative diagnosis of neuroendocrine tumor (NET) was made, and the patient underwent a pancreaticoduodenectomy along with resection of the spleen.

Macroscopically, polypoid whitish solid tumor with intratumoral hemorrhage, predominantly around the head of the pancreas, was noted within MPD (Fig. 4A and B). Histopathologically, the tumor was composed of a proliferation of mononuclear cells and multinucleated giant cells, admixed with hemosiderin deposits (Fig. 4C). There was a small ductal adenocarcinoma component as well. The tumor was located predominantly within the intraluminal space of MPD, associated with microscopic invasive foci to the parenchyma at the body of the pancreas (Fig. 4B). Immunohistochemical examination revealed multinucreated giant cells positive for CD68 staining. CD31 staining revealed abundant vascular space in the tumor. Ductal adenocarcinoma component was positive for MUC1, AB-PAS, and Cytokeratin 7. The final diagnosis of undifferentiated carcinoma of the pancreas with osteoclast-like giant cells (UCPOGC), T1N0M0, was thus made.

The patient received adjuvant chemotherapy with Tegafur, Gimeracil, and Oteracil Potassium (as known as TS-1) for 1 year. She is alive without evidence of local recurrence or distant metastasis 35 months after the surgery at the time of this writing.

Discussion

UCPOGC is a very rare tumor accounting for 2%-7% of all pancreatic cancers [1]. UCPOGC is initially described in 1968 by Juan Rosai as a variant of undifferentiated carcinoma [2]. Unlike the original undifferentiated carcinoma, which is very

Fig. 1 – Dynamic CT using total volume of 600 mg/kg iodine contrast medium, injected in 30 seconds. (A) Arterial phase transaxial image obtained 40 seconds after the commencement of contrast medium injection at the level of the lesion of the pancreatic body. Note a tubular lesion in the main pancreatic duct of the pancreatic body with homogeneous enhancement (arrow). (B) Atrial phase transaxial image at the level of the pancreatic head. The lesion shows less enhancement (arrow) as compared to (A). Thickened gallbladder wall with calcification (arrowhead) turned out to be adenomyomatosis at the surgery. (C) Equilibrium phase obtained 240 seconds after the commencement of contrast medium injection. The lesion shows apparent washout (arrow) and atrophied pancreas parenchyma of the pancreatic tail shows relatively strong enhancement to the normal pancreatic parenchyma, which indicates chronic obstructive pancreatitis (arrow heads).
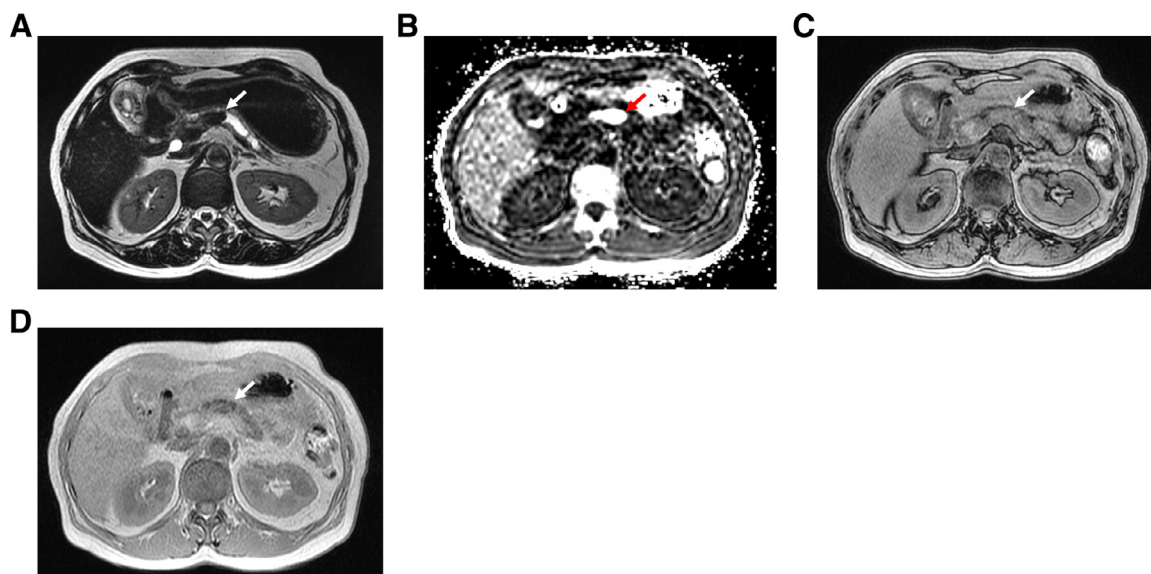
Fig. 2 – Magnetic resonance (MR) imaging of the pancreas. (A) Heavily T2-weighted image (repetition time [TR]/echo time [TE] = 6000/259.8 milliseconds). The pancreas lesion is illustrated as a hypointense nodule (arrow). Main pancreatic duct of the pancreas tail is dilated. (B) R2* map generated from IDEAL-IQ (TR/TE/FA = 7.4/3.2ms/3°, echo space 0.9, 3 echoes × 2). The lesion is depicted as a very hyperintense nodule. (C) Gradient-echo 2D T1-weighted out-of-phase chemical shift image (TR/TE/FA = 220.0/1.2/50°). The lesion shows intermediate to high signal intensity (arrow). (D) Gradient-echo 2D T1-weighted in-phase chemical shift image (TR/TE/FA = 220.0/2.5/50°). Apparent signal loss is seen in the lesion (arrow).
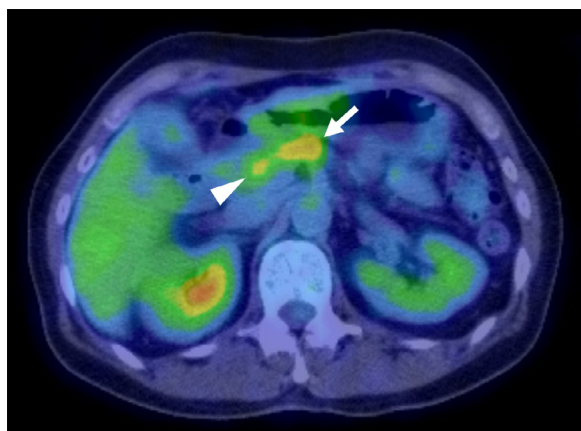
Fig. 3 – Fluorine 18 Fluorodeoxyglucose (^{18}FDG) positron emission tomography-computed tomography (PET-CT). Transaxial image through the level of the pancreas lesion. ^{18}FDG uptake is increased in the lesion of the pancreatic body (arrow) and head (arrow head). The maximum standardized uptake value of the pancreas mass was 4.03. No other abnormal FDG uptake was seen.

aggressive and frequently metastasizes to lymph nodes or other organs, UCPOGC is known to be less aggressive, the prognosis of which is better than invasive ductal carcinoma of the pancreas [3]. Clinical presentation of UCP is nonspecific, including abdominal pain, a palpable mass, weight loss, etc, and tumor markers including CA 19-9 elevate in about half of the patients [4,5]. UCPOGC is usually large, moderately to highly hypervascular, and exophytic tumors with large areas of

intratumoral necrosis and hemorrhage [4,6,7]. Especially, intratumoral hemorrhage is often observed even if the tumor size is small [2].

In our case, R2* map obtained from IDEAL IQ clearly revealed this hemorrhagic nature of this small lesion. IDEAL-IQ (GE, Milwaukee, WI) is a newly developed multiecho 3D Dixon's method, with which quantitative fat image and R2* map can be simultaneously obtained under breath-holding, by means of correcting several confounding factors including T2* decay, T1 bias, B0 inhomogeneity, eddy currents, and multipeak fat spectra [8–12]. Because iron is the most common substance that causes R2* elevation or T2* shortening, high signal on R2* map is indicative of the presence of hemosiderin [9–12], a degraded substance of hemorrhage. Similar observation has recently been reported using T2*-weighted images for this entity [14]. This elevated R2* is considered the cause of hypointensity of the lesion on diffusion-weighted images, whereas there was apparent accumulation of FDG at the lesion on PET/CT.

Another point in our case was the intraluminal growth pattern of the tumor without macroscopic parenchymal component. To the best of our knowledge, 4 cases of small UCPOGCs with predominant intraductal growth and without macroscopic extraductal mass formation have been reported [1,3,6,15]. Recently, Muraki et al revealed that UCPOGC often show intraductal growth pattern (40%), which may suggest relatively indolent biological behavior of this entity [3,7]. Differential diagnosis of tumors exhibiting this peculiar growth pattern includes intraductal papillo-tubular neoplasm, and intraductal papillary mucinous neoplasms (MD type), and NET, but small number of cases of acinar cell carcinoma and UCPOGC have been reported as well
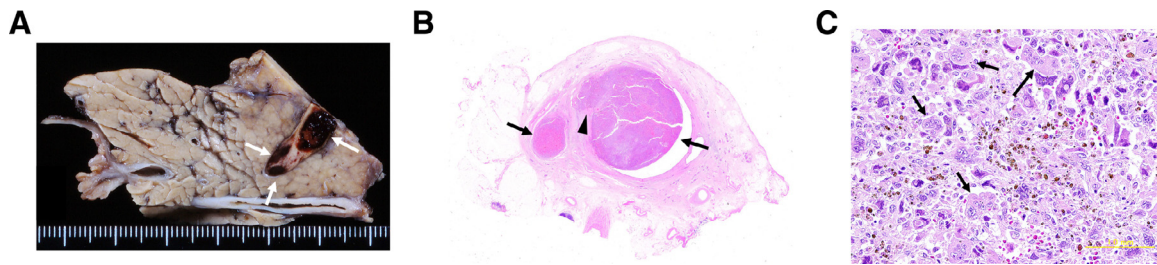
Fig. 4 – Histopathological and macroscopic findings. (A) A gross appearance of the cut surface along the main pancreatic duct (MPD). A whitish lesion with intratumoral hemorrhage (arrows) is noted occupying the lumen of MPD. (B) H&E staining with low magnification shows the tumor protruding into the MPD lumen (arrows) and shows small tumor invasion to the surrounding parenchyma (arrowheads). (C) H&E staining with high magnification shows highly atypical mononuclear cells and multinuclear giant cells (arrows) with admixed hemosiderin (small brownish nodules).

[1,3–5,15–17]. Because the lesion in the current report was apparently hypervascular, our preoperative diagnosis of NET was made. NET, however, usually grows into MPD continuously from distinct parenchymal primary lesion (namely, as tumor thrombus) and its intraductal component tends to show high signal intensity on T2-weighted images [18,19,13], which is discordant with the present case.

Although R2* map is a useful tool to detect small amount of iron, it is based on sophisticated technology and is not necessarily available in every institute. On the other hand, chemical shift gradient-echo imaging is a basic sequence in clinical practice, and is now widely available. Because the echo time of the in-phase image is set longer than that of the out-of-phase image, significant signal loss on the in-phase image as compared to the out-of-phase image indicates T2* shortening effect, typically caused by the presence of iron deposits [20]. Actually this finding was confirmed in our case as well, and therefore, we believe this is a good and easy alternative to R2* map in routine clinical practice.

In conclusion, radiologists should include UCPOGC in the differential diagnosis of intraluminal lesions located within MPD, particularly when its hemorrhagic nature is suggested on imaging, including R2* map.

REFERENCES

[1] Tezuka K, Yamakawa M, Jingu A, Ikeda Y, Kimura W. An unusual case of undifferentiated carcinoma in situ with osteoclast-like giant cells of the pancreas. Pancreas 2006;33(3):304–10.

[2] Rosai J. Carcinoma of pancreas simulating giant cell tumor of bone. Electron-microscopic evidence of its acinar cell origin. Cancer 1968;22:333–44.

[3] Ishii S, Kobayashi G, Fujita N, Noda Y, Ito K, Horaguchi J, et al. Undifferentiated carcinoma of the pancreas involving intraductal pedunculated polypoid growth. Intern Med 2012;51:3373–7. doi:10.2169/internalmedicine.51.8779.

[4] Muraki T, Reid MD, Basturk O, Jang KT, Bedolla G, Bagci P, et al. Undifferentiated carcinoma with osteoclastic giant cells of the pancreas: clinicopathological analysis of 38 cases highlights a more protracted clinical course than currently appreciated. Am J Surg Pathol 2016;40(9):1203–16.

[5] Matsumura Y, Iwai K, Kawasaki R, Matsui A. A case of spontaneously ruptured anaplastic carcinoma (giant cell type) of the pancreas with intraabdominal hemorrhage. Jpn J Gastroenterol Surg 2007;40:456.

[6] Naito Y, Kinoshita H, Okabe Y, Arikawa S, Higashi K, Yamasaki F, et al. Pathomorphologic study of undifferentiated carcinoma in seven cases: relationship between tumor and pancreatic duct epithelium. J Hepatobiliary Pancreat Surg 2009;16:478–84.

[7] Ichikawa T, Federle MP, Ohba S, Ohtomo K, Sugiyama A, Fujimoto H, et al. Atypical exocrine and endocrine pancreatic tumors (anaplastic small cell, and giant cell types): CT and pathologic features in 14 patients. Abdom Imaging 2000;25(4):409–19.

[8] Reeder SB, Prineda AR, Wen Z, Shimakawa A, Yu H, Brittain JH, et al. Iterative decomposition of water and fat with echo asymmetry and least squares estimation (IDEAL): application with fast spin-echo imaging. Magn Reson Med 2005;54:636–44.

[9] Wood JC, Enriquez C, Ghugre N, Tyzka JM, Carson S, Nelson MD, et al. MRI R2 and R2* mapping accurately estimates hepatic iron concentration in transfusion-dependent thalassemia and sickle cell disease patients. Blood 2005;106(4):1460–5.

[10] Ghugre NR, Coates TD, Nelson MD, Wood JC. Mechanisms of tissue–iron relaxivity: nuclear magnetic resonance studies of human liver biopsy specimens. Magn Reson Med 2005;54(5):1185–93. doi:10.1002/mrm.20697.

[11] Shinohara Y, Kato A, Yamashita E, Ogawa T. R2* Map by IDEAL IQ for acute cerebral infarction: compared with susceptibility vessel sign on T2*-weighted imaging. Yonago Acta Medica 2016;59:204–9.

[12] Nishiyama M, Sakamoto K, Shinagawa Y, Morita A, Urakawa H, Fujimitsu R, et al. A case of porphyria cutanea tarda of the liver exhibiting multifocal macrovesicular steatosis, probably caused by uneven iron accumulation. Abdom Radiol 2017;42:1813–18. doi:10.1007/s00261-017-1056-0.

[13] Fukukura Y, Kumagae Y, Hirahara M, Hakamada H, Nagano H, Nakajo M, et al. CT and MRI features of undifferentiated carcinomas with osteoclast-like giant cells of the pancreas: a case series. Abdom Radiol 2019;44:1246–55.

[14] Kawai Y, Nakamichi R, Noriko K, Miyake H, Fujino M, Itoh S . A case of undifferentiated carcinoma of the pancreas mimiching main-duct intraductal papillary mucinous neoplasm (IMPN). Abdom Imaging 2014;40:466–70. doi:10.1007/s00261-014-0326-3.

[15] Nishimura M, Wada H, Eguchi H, Iwagami Y, Yamada D, Asaoka T, et al. A case report of acinar cell carcinoma of pancreas with extensive intraductal growth to the branch-main pancreatic duct. Jpn J Cancer Chemother 2017;44(12):1568–70.

[16] Askan G, Bagci P, Memis B, Basturk O. Intraductal neoplasms of the pancreas: an update. Turk Patoloji Derg 2017;33:87–102.

[17] Kiyonaga M, Matsumoto S, Mori H, Yamada Y, Takaiji R, Hijiya N, et al. Pancreatic neuroendocrine tumor with extensive intraductal invasion of the main pancreatic duct: a case report JOP. J Pancreas 2014;15(5):497–500.

[18] Inagaki M, Watanabe K, Yoshikawa D, Suzuki S, Ishizaki A, Matsumoto K, et al. A malignant nonfunctioning pancreatic endocrine tumor with a unique pattern of intraductal growth. J Hepatobiliary Pancreat Surg 2007;14:318–23.

[19] Shimizu K, Shiratori K, Toki F, Suzuki M, Imaizumi T, Takasaki K, et al. Nonfunctioning islet cell tumor with a unique pattern of tumor growth. Dig Dis Sci 1999;44:547–51.

[20] Yoshimitsu K, Kakihara D, Irie H, Tajima T, Nishie A, Asayama Y, et al. Papillary renal carcinoma: diagnostic approach by chemical shift gradient-echo and echo-planar MR imaging. J Magn Reason Imaging 2006;23:339–44.